New Astronomy 14 (2009) 97–108

Contents lists available at ScienceDirect

New Astronomy

journal homepage: www.elsevier.com/locate/newast

CCD Washington photometry of three highly field star contaminated open clusters in the third Galactic quadrant

A.E. Piatti [a,*], J.J. Clariá [b], M.C. Parisi [b], A.V. Ahumada [b]

[a] Universidad Nacional de Córdoba, Instituto de Astronomía y Física del Espacio, CC 67, Suc. 28, 1428 Ciudad de Buenos Aires, Argentina
[b] Observatorio Astronómico, Universidad Nacional de Córdoba, Laprida 854, 5000 Córdoba, Argentina

ARTICLE INFO

Article history:
Received 26 February 2008
Received in revised form 22 May 2008
Accepted 27 May 2008
Available online 4 June 2008
Communicated by F.D. Macchetto

Keywords:
Galaxy: open clusters and associations: general
Galaxy: open clusters and associations: individual: (Czernik 26, Czernik 30, Haffner 11)
Techniques: photometric
Galaxies: dwarf

ABSTRACT

We present CCD photometry in the Washington system C and T_1 passbands down to $T_1 \sim 19.5$ magnitudes in the fields of Czernik 26, Czernik 30, and Haffner 11, three poorly studied open clusters located in the third Galactic quadrant. We measured T_1 magnitudes and $C - T_1$ colors for a total of 6472 stars distributed throughout cluster areas of $13.6' \times 13.6'$ each. Cluster radii were estimated from star counts in appropriate-sized boxes distributed throughout the entire observed fields. Based on the best fits of isochrones computed by the Padova group to the ($C - T_1$, T_1) color-magnitude diagrams (CMDs), we derived color excesses, heliocentric distances and ages for the three clusters. These are characterized by a relatively small angular size and by a high field star contamination. We performed a firm analysis of the field star contamination of the CMDs and examined different relationships between the position in the Galaxy of known open clusters located within 1 kpc around the three studied ones, their age and their interstellar visual absorption. We confirm previous results in the sense that the closer the cluster birthplace to the Galactic plane, the higher the interstellar visual absorption. We also found that the space velocity dispersion perpendicular to the Galactic plane diminishes as the clusters are younger. The positions, interstellar visual absorptions, ages, and metallicities of the three studied clusters favor the hypothesis that they were not born in the recently discovered Canis major (CMa) dwarf galaxy before it was accreted by the Milky Way.

1. Introduction

Galactic open clusters (OCs) have long been considered unrivalled objects not only to undertake structural and evolutionary studies of our Galaxy's disc but also to trace its chemical evolution. Because their ages, distances, and metallicities can be estimated with fairly good accuracy and because they can be seen at large distances from the Sun, their fundamental parameters constitute excellent tracers to the structure and chemical evolution of the Galactic disc. OCs are also tracers to many other important disc properties such as the age-metallicity relationship, the disc age and so on. Although the number of studied OCs recently increased significantly, nearly 60% of the ~1700 Galactic OCs known to exist (Dias et al., 2002) are still unstudied objects. To examine how the disc properties evolved in time, we must improve the statistics of well-studied OCs. In fact, the greater the number of OCs with well determined distances, ages and metallicities, the more precise and detailed the analysis of the structure and the metal abundance gradient in the Galactic disc as well as their evolution over time.

The CCD CT_1 photometric data reported in this study were obtained as part of a project that is still being developed at the Observatorio Astronómico de Córdoba (Argentina). This project aims at determining the basic parameters or at refining the quality of observationally determined properties for some unstudied or poorly studied OCs, located in different regions of the Milky Way. We have favored the observation of clusters which are interesting not only because of the derivation of their fundamental parameters, but also for the number of red giant candidates they contain as well as for the possibilities they provide in terms of cluster metal content derivation (see e.g. Piatti et al., 2003; Piatti et al., 2004).

In the current study we discuss CT_1 photometry of three low-contrast Galactic OCs, namely Czernik 26, Czernik 30 and Haffner 11 – also known as BH 3 (van den Bergh and Hagen, 1975) or ESO 429-3 (Lauberts, 1982) – which are located in the third Galactic quadrant. Equatorial and Galactic coordinates of target clusters are given in Table 1. No photometry was reported so far for these objects. Only Haffner 11 has been recently studied by Bica and Bonatto (2005) using 2MASS data. They applied a statistical field star decontamination procedure to infer on the intrinsic color-magnitude diagram (CMD) morphology, which is critical for such low-contrast object. Bica and Bonatto (2005) derived $E(B-V) = 0.36 \pm 0.03$, a heliocentric distance of 5.2 ± 0.2 kpc and an age of

* Corresponding author. Tel.: +54 351 4331064; fax: +54 351 4331063.
E-mail address: andres@iafe.uba.ar (A.E. Piatti).

1384-1076/$ - see front matter © 2008 Elsevier B.V. All rights reserved.
doi:10.1016/j.newast.2008.05.006

Table 1
Observation log of selected clusters

Star cluster	α_{2000} (hms)	δ_{2000} (°′″)	l (°)	b (°)	Filter (s)	Exposure	Airmass	Seeing (″)
Czernik 26	063048	−041300	214.347	−6.508	C	300	1.130	1.35
					C	300	1.135	1.35
					R	30	1.150	1.20
					R	30	1.151	1.15
Czernik 30	073118	−095800	226.369	4.173	R	30	1.067	1.00
					R	30	1.067	1.15
					C	300	1.069	1.50
					C	300	1.071	1.45
Haffner 11	073525	−274300	242.395	−3.544	R	60	1.024	1.20
					R	60	1.026	1.25
					C	400	1.031	1.45
					C	400	1.040	1.55

0.9 ± 0.2 Gyr. Using the K magnitude of the He-burning red clump from 2MASS photometry, Bellazzini et al. (2006) obtained a larger reddening value, i.e. $E(B-V) = 0.57$ and a heliocentric distance of 5.5 ± 0.8 kpc.

This paper is organized as follows. Section 2 describes the observational material and the data reduction. In Section 3, we describe the main features of the $(C-T_1, T_1)$ CMD as well as some structural cluster features We also determine in this section the cluster fundamental parameters through the fitting of theoretical isochrones computed for the Washington system. In Section 4 we compare the properties here derived for Czernik 26, Czernik 30 and Haffner 11 with those of OCs with known basic parameters projected in nearly the same direction. We also analyze in this section the possible association of the three studied clusters with the CMa galaxy. Section 5 contains a summary of our main conclusions.

2. Observations and reductions

The observational setup and the stellar photometry procedure are identical to those used in Clariá et al. (2007). To sum up, the CCD images were obtained using the 0.9 m telescope at Cerro Tololo Inter-American Observatory (CTIO, Chile), equipped with the 2048 × 2048 pixel Tektronix 2K No. 3 CCD, during the night of 19–20 December, 2004. Observations were carried out with the Washington C and Kron-Cousins R filters (Canterna, 1976). The latter has a significantly higher through-put as compared with the Washington T_1 filter so that R magnitudes can be accurately transformed to yield T_1 magnitudes (Geisler, 1996). The CCD camera has a field-of-view of 13.6′ × 13.6′ with a plate scale of 0.4″/pixel. Table 1 shows the log of the observations with filters, exposure times, airmasses, and seeing estimates. All the data were taken under photometric conditions. Standard stars from the list of Geisler (1996) were observed in order to secure the transformation from the instrumental to the standard system. The instrumental signatures (e.g. the bias level and pixel-to-pixel sensitivity variations) in the CCD images were removed by using standard observational techniques and tasks in IRAF.

The stellar photometry was performed using the star-finding and point-spread-function (PSF) fitting routines in the DAOPHOT/ALLSTAR suite of programs (Stetson et al., 1990). Radially varying aperture corrections were applied to remove the effects of PSF variations across the field-of-view, although a quadratically-varying PSF was employed. The resulting instrumental magnitudes were standardized using Eqs. (1) and (2) from Clariá et al. (2007). The root-mean-square deviations of the fitted values to the standard stars were all less than 0.025 magnitudes. Tables 2–4 present the final photometry of the three clusters. Magnitude and color errors are the standard deviations of the mean or the observed photometric errors for stars with only one measurement. Only fragments of these tables are presented here as guidance, regarding their forms and contents. The complete tables, however, are available on the on-line version of the journal.

3. Cluster fundamental parameters from color-magnitude diagram features

Fig. 1 shows the $(C-T_1, T_1)$ CMDs for all the observed stars in the three cluster fields. All the cluster CMDs are profusely contaminated by field stars. As seen in the three panels of Fig. 1, it is difficult to identify the cluster main sequences with precision. Note that we are not dealing with heavily reddened cluster fields, since the observed stars mostly have $C-T_1$ colors between 1 and 2.5 magnitudes. We do not deal with densely crowded fields either because we have only measured from 1 up to 2.5 thousand stars per field. We are simply considering relatively compact and low populated open clusters projected onto comparatively more dense star fields.

With the aim of disentangling cluster features from those belonging to their surrounding fields, we started by determining the location of the cluster centers in order to construct stellar density profiles. These would help to adopt the optimum cluster radii. This straightforward approach allows us to obtain CMDs dominated by cluster stars, although some field star contamination is unavoidable. The success of this method depends on the ratio between the number of cluster stars and the number of field stars within each radius. We have here refined our techniques and used a more quantitative and definite analysis than that used in our previous works in this series. It is worth mentioning that we did not succeed in our attempt to fit the well-known empirical model of King (1962) to the observed density profiles of our OC sample. As Piskunov et al. (2008) found, King's model does not successfully work for OCs having a low number of members, because that causes uncertainties in the observed density profiles. Furthermore, since the spatial boundaries of the observed clusters are not clearly defined and the proportion of field stars projected on the cluster area is relatively high, the King's fit based on the inner area becomes less reliable. It can also lead to a significant bias in the resulting core radii. On the other hand, if we consider the behavior of the density profile in the outer regions and even outside the cluster limits, the tidal radii would also result to be somewhat uncertain.

The coordinates of the cluster centers and their estimated uncertainties were determined by fitting Gaussian distributions to the star counts in the x and y directions for each cluster. The fits of the Gaussians were performed using the NGAUSSFIT routine in the STSDAS/IRAF package. We adopted a single Gaussian and fixed the constant to the corresponding background levels (i.e. stellar

Table 2
CCD CT_1 data of stars in the field of Czernik 26

Star	x (pixel)	y (pixel)	T_1 (magnitude)	$\sigma(T_1)$ (magnitude)	$C-T_1$ (magnitude)	$\sigma(C-T_1)$ (magnitude)	n
11	1039.030	15.874	16.009	0.019	4.024	0.017	2
12	682.733	16.490	16.708	0.055	2.955	0.028	2
13	1721.936	17.064	15.030	0.069	4.401	0.011	2
–	–	–	–	–	–	–	–
–	–	–	–	–	–	–	–

Note: (x, y) coordinates correspond to the reference system of Fig. 3.

Table 3
CCD CT_1 data of stars in the field of Czernik 30

Star	x (pixel)	y (pixel)	T_1 (magnitude)	$\sigma(T_1)$ (magnitude)	$C-T_1$ (magnitude)	$\sigma(C-T_1)$ (magnitude)	n
245	1132.423	357.316	15.821	0.017	1.184	0.040	2
246	384.038	357.691	16.231	0.001	1.184	0.007	2
247	82.463	358.485	17.201	0.025	1.645	0.015	2
–	–	–	–	–	–	–	–
–	–	–	–	–	–	–	–

Note: (x, y) coordinates correspond to the reference system of Fig. 5.

Table 4
CCD CT_1 data of stars in the field of Haffner 11

Star	x (pixel)	y (pixel)	T_1 (magnitude)	$\sigma(T_1)$ (magnitude)	$C-T_1$ (magnitude)	$\sigma(C-T_1)$ (magnitude)	n
437	610.867	465.929	17.401	0.022	2.082	0.010	2
438	1582.931	466.631	18.087	0.000	1.774	0.031	2
439	1970.034	468.186	14.233	0.008	0.979	0.007	2
–	–	–	–	–	–	–	–
–	–	–	–	–	–	–	–

Note: (x, y) coordinates correspond to the reference system of Fig. 6.

field densities assumed to be uniform) and the linear terms to zero. The center of the Gaussian, its amplitude and its full width at half-maximum (FWHM) acted as variables. The number of stars projected along the x and y directions were counted within intervals of 50 pixel wide. In addition, we checked that using spatial bins from 25 to 50 pixels or from 50 to 100 pixels does not result in significant changes in the derived centers. We iterated the fitting procedure on average once, after eliminating a couple of discrepant points. Cluster centers were finally determined with a typical standard deviation of ±10 pixels ($\sim 4''$) in all cases.

With the aim of tracing the cluster morphologies more closely, we treated the data taking into account the possibility of their being elliptically shaped. We made use of the N2GAUSSFIT program in the STSDAS/IRAF PACKAGE, which allows a two-dimensional elliptical Gaussian fit represented by the Gaussian amplitude, the x and y centers, the FWHMs, the ellipticity, the position angle and the background level. We selected the deepest images of Czernik 26, Czernik 30 and Haffner 11 and kept all seven coefficients so that they could be varied during the fit. After few iterations varying the size of the windows which defined the fitted areas, we derived the best values of the seven coefficients based on the smallest obtained chi-square, rms and individual coefficient errors.

The background levels and the x and y centers showed excellent agreement with those derived before for our three studied clusters, the ellipticity being around 0.1 in every case. The top left panel of Figs. 3–5 shows the schematic finding chart of each cluster, in which the sizes of the plotting symbols are proportional to the T_1 brightness of the stars. We also drew three concentric circles corresponding to $r_{\rm FWHM}$, $r_{\rm clean}$, and $r_{\rm field}$ (see below more details), respectively. We overplotted in blue the corresponding ellipse obtained from the two-dimensional Gaussian fit. As can be seen in Figs. 3–5, no relevant difference was found that allows to improve the cleaning of the cluster CMDs. We think that this method would be worth applying in the cases of not only more populated and regular-shaped clusters but also in those projected onto comparatively less dense star fields. Unfortunately, we are not dealing with clusters of such characteristics.

We then constructed the cluster radial profiles based on star counts within boxes of 50 pixels a side distributed throughout the whole field of each cluster. The selected size of the box allowed us to sample statistically the star spatial distribution and to avoid spurious effects mainly caused by the presence of localized groups, rows or columns of stars. Thus, the number of stars per unit area at a given radius r can be directly calculated through the expression

$$(n_{r+25} - n_{r-25})/((m_{r+25} - m_{r-25}) \times 50^2), \quad (1)$$

where n_j and m_j represent the number of stars and boxes included in a circle of radius j, respectively. Note that this method does not necessarily require a complete circle of radius r within the observed field to estimate the mean stellar density at that distance. This is an important consideration since having a stellar density profile which extends far away from the cluster center allows us to estimate the background level with high precision. This is necessary to derive the cluster radius, defined as the distance from the cluster center where the stellar density profile intersects the background level. It is also helpful to measure the FWHM of the stellar density profile, which plays a significant role – from a stellar content point of view – in the construction of the cluster CMDs. Besides, it helps to estimate the percentage of field contamination.

The resulting density profiles expressed as number of stars per unit area in arcmin^2 are shown in Fig. 2. In that figure, we illustrate the region around the center of each cluster up to $7'$. The background region of each cluster was delimited by the observed field boundaries and by a circle of $6'$ radius from the cluster's center. The errorbars in the figure represent the uncertainties estimated at

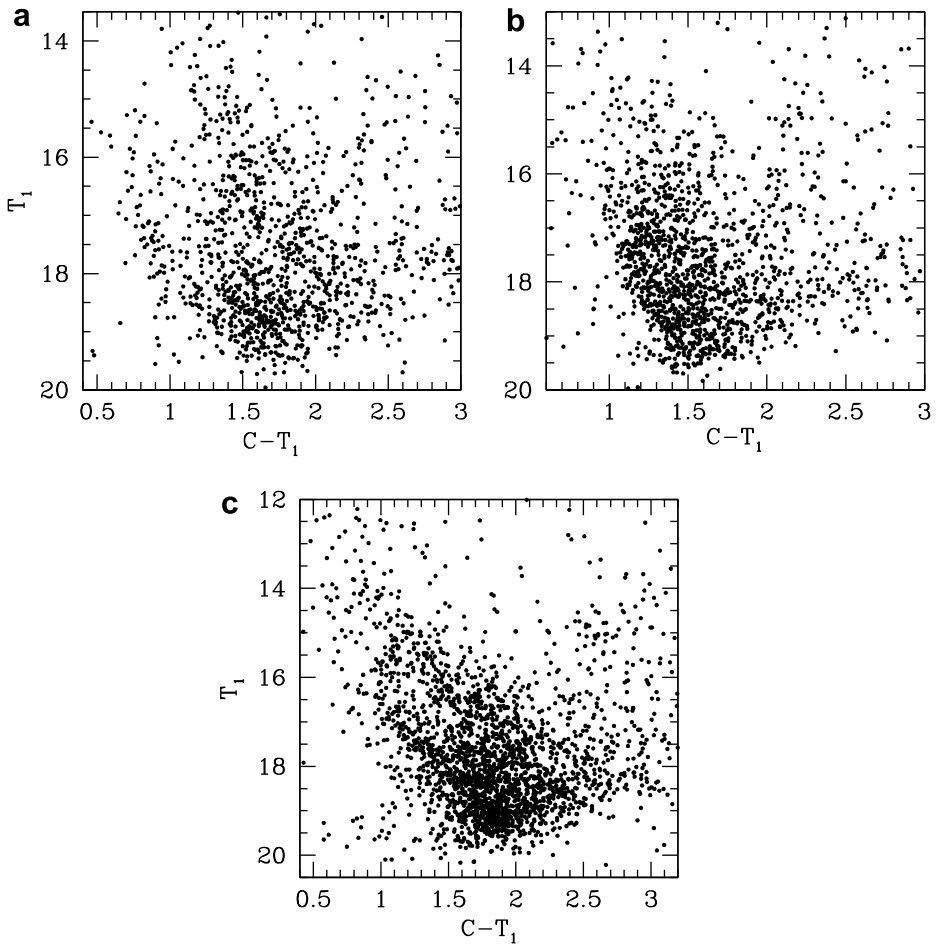

Fig. 1. $(C - T_1, T_1)$ CMD for stars observed in the field of: (a) Czernik 26; (b) Czernik 30; and (c) Haffner 11.

various distances from the centers. Each errorbar was fixed by comparing two additional radial profiles to those shown in Fig. 2. Such additional profiles were constructed following the steps described above but using boxes of 25 and 100 pixels a side, respectively. This was done to take into account the effects of using spatial bins of different sizes. It is observed that the more inwards a radius, the longer the errorbars. This may be due to the non-uniform distribution of cluster stars. Table 5 lists the calculated background levels, the radii at the FWHM ($r_{\rm FWHM}$), the estimated radii which yield the best enhanced cluster fiducial features ($r_{\rm clean}$), the cluster radii ($r_{\rm cls}$), and the field contamination estimated in percentage for different radial intervals. Note that the percentage of field stars is relatively high, even for $r < r_{\rm FWHM}$, and rapidly increases outwards from the cluster core regions, indicating the relatively small sizes of the clusters. No cluster stands out clearly over its surrounding field at a radial range from $r_{\rm FWHM}$ to $r_{\rm clean}$.

We constructed three CMDs covering different circular extractions around each cluster as shown in Figs. 3–5. The panels in the figures are arranged, from left to right and from top to bottom, in such a way that exhibit the stellar population variations from the innermost to the outermost regions of the cluster fields. We start with the CMD for stars distributed within $r < r_{\rm FWHM}$, followed by that of the cluster regions delimited by $r < r_{\rm clean}$ and finally by the adopted field CMDs.

In order to build optimum cluster CMDs, which result from a compromise between maximizing the number of cluster stars and minimizing the field star contamination, we performed different circular extractions around every cluster center. We used the CMDs corresponding to the stars within $r_{\rm FWHM}$ as the cluster fiducial sequence references. Then, we varied the distance from the cluster centers starting at $r_{\rm FWHM}$ and built different series of extracted CMDs. Finally, we chose those CMDs – one per cluster – which maximize the star cluster population and minimize the field star contamination in the CMDs. Notice that fitting a King's stellar density profile to our own cluster profiles does not improve the cluster radii estimates, if we consider them from a meaningful physical point of view. What is more, we believe that it would be necessary to inspect closely each extracted CMD to decide which radius better depicts the cluster features in these highly contaminated star fields.

The main cluster features can be identified by inspecting Figs. 3–5 (left bottom panels). What first attracts our attention is that the three cluster main sequences (MSs), which look well populated, show clear signs of evolution. With the exception of Czernik 30 whose MS develops along ~3.0 magnitudes, the remaining MSs extend along ~4.5 magnitudes. In addition, the evident hook at the MS turnoff of Czernik 30's CMD and the red giant clumps centered at $T_1 \sim 14.5$–15.0 and $C - T_1 \sim 2.4$–2.6 magnitudes in the CMDs of Czernik 30 and Haffner 11, are clear hints that we are dealing with intermediate-age or old open clusters. Note that all these red giant clump stars are distributed within $r < r_{\rm clean}$, while several of them are located even within $r < r_{\rm FWHM}$. The width of the clusters' MSs does not appear to be due to photometric errors, since these hardly reach a tenth of magnitude at any T_1 level. Therefore, such width could be caused by intrinsic effects (evolution, binarity, etc.), by differential reddening and/or by field star contamination. Notice

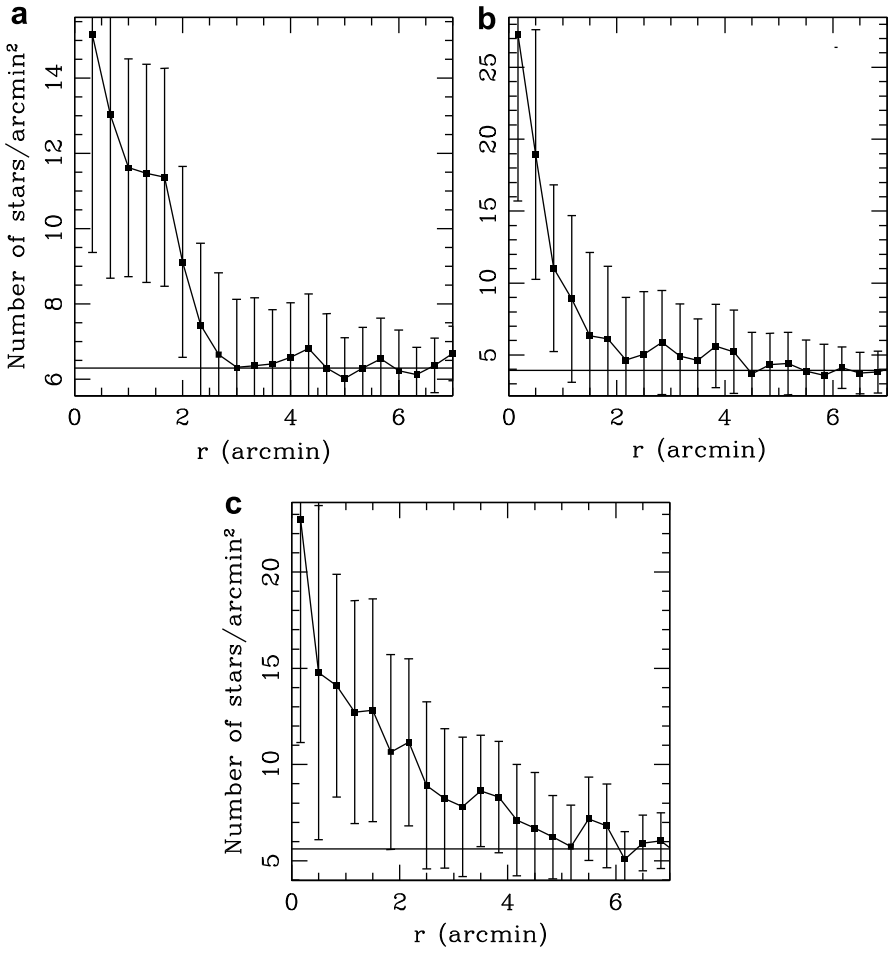

Fig. 2. Stellar density radial profile centered on the cluster for stars observed in the field of: (a) Czernik 26; (b) Czernik 30; and (c) Haffner 11. The horizontal lines represent the measured background levels (see Section 3 for details).

Table 5
Cluster sizes and field contamination

Name	Background (star/armin^2)	r_{FWHM} (pixel)	r_{clean} (pixel)	r_{cls} (pixel)	Field contamination (%)		
					$r < r_{FWHM}$	$r_{FWHM} < r < r_{clean}$	$r_{clean} < r < r_{cls}$
Czernik 26	6.30 ± 0.45	150	350	400	54	67	88
Czernik 30	3.94 ± 0.56	90	200	650	25	44	70
Haffner 11	5.62 ± 0.45	100	300	700	38	50	71

that field stars also have magnitudes and colors different from those of the clusters' MSs. This fact can be observed if we compare the right (field) with the left (cluster) bottom panels in Figs. 3–5. In the subsequent analysis, we will use the CMDs with $r < r_{clean}$ for all the clusters.

From the cluster CMDs, we estimated the cluster color excesses $E(C-T_1)$, their metallicities [Fe/H] and their distance moduli, and then fitted theoretical isochrones from the Padova group to each cluster CMD to estimate the cluster's age. We used the isochrones computed by Girardi et al. (2002), which include overshooting effect. They are available in steps of $\Delta\log t = 0.05$ dex. As shown in previous studies (Piatti et al., 2003; Piatti et al., 2007), these isochrones lead to results similar to those derived from the Geneve group's isochrones (Lejeune and Schaerer, 2001). However, they reach larger magnitudes, thus allowing a better fit to the cluster fainter portions of the MSs. To estimate all these parameters we proceeded as follows: firstly, we selected zero-age main sequences (ZAMSs) with $Z = 0.008$, 0.019, and 0.040 ([Fe/H] = −0.4, 0.0, and +0.3), which cover the metallicity range of most of the Galactic open clusters studied in detail (Mermilliod and Paunzen, 2003). Next, we fitted these ZAMSs to the cluster CMDs to derive color excesses and apparent distance moduli for each selected metallicity. Then, using each of the derived $(E(C-T_1), T_1-M_{T_1})_{[Fe/H]}$ sets, we performed isochrone fits. We repeated the fits for a large number of isochrones covering appropriate age ranges according to each cluster. The brightest magnitude in the MS, the bluest point of the turnoff and the locus of the red giant clump (when visible), were used as reference points during the fits. Finally, we chose the best fit for each $(E(C-T_1), T_1-M_{T_1})_{[Fe/H]}$ set and compared all the individual best fits to choose the one which best reproduced the cluster features. Fig. 6 illustrates the results of our task, while Table 6 lists the estimated $E(B-V)$ color excess, distance from the Sun (d), age and metallicity of the clusters. Their errors were derived bearing in mind the broadness of the cluster MSs and, in the case of the cluster distances, the expression $0.46 \times [\sigma(V-M_V) + 3.2 \times \sigma(E(B-V))] \times d$, where $\sigma(V-M_V)$ and

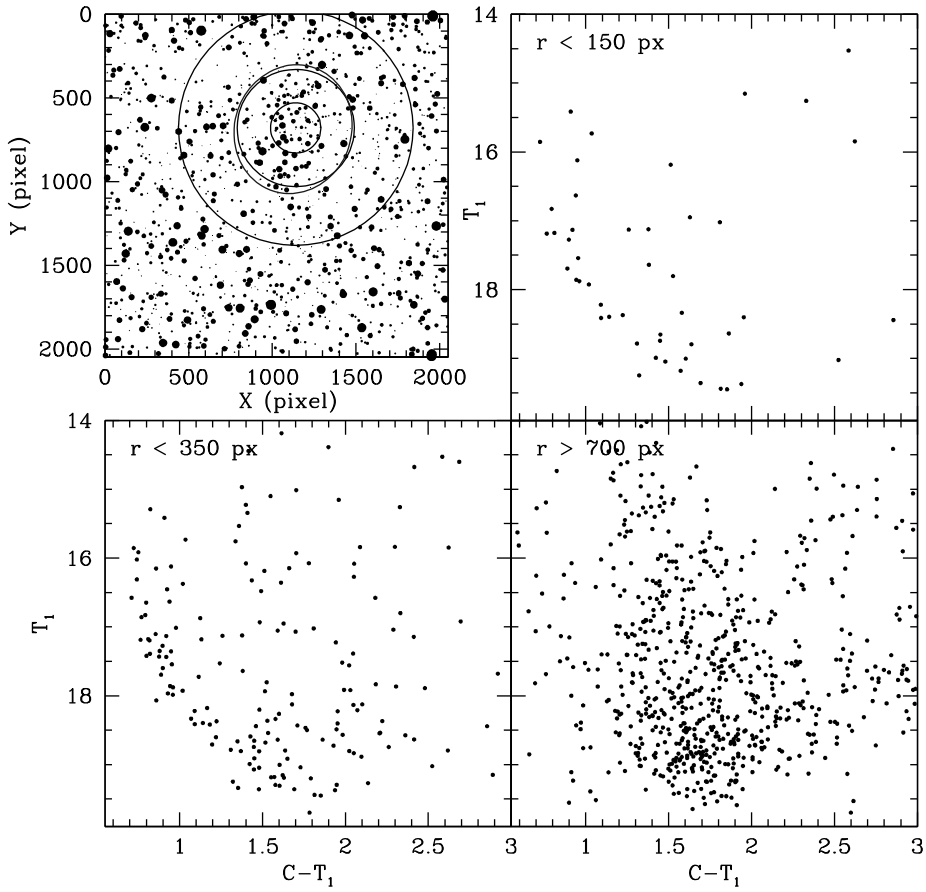

Fig. 3. Schematic finding chart of the stars observed in the field of Czernik 26 (upper left), with three concentric circles corresponding to the extracted CMDs, for: $r < r_{FWHM}$ (upper right), $r < r_{clean}$ (bottom left), and $r > r_{field}$ (bottom right). The blue ellipse overplotted in the finding chart corresponds to the result obtained from the two-dimensional Gaussian fit. North is up and east is to the left.

$\sigma(E(B-V))$ represent the estimated errors in $V-M_V$ and $E(B-V)$, respectively. The expressions $E(C-T_1) = 1.97E(B-V)$ and $M_{T_1} = T_1 + 0.58E(B-V) - (V-M_V)$ Geisler (1996) were used to relate both color excesses and distance moduli. Note that our $E(B-V)$ value for Haffner 11 is identical to that inferred by Bellazzini et al. (2006), while the heliocentric distance we obtained also coincides – within the involved errors – with their distance value.

4. Implications on the Galactic disc features

The three selected OCs are located in the third Galactic quadrant ($\langle l \rangle = 229°$), on approximately the same solar centered circle of radius ~6.5 kpc. They span a Galactic longitude range $\Delta l = \pm 15°$ and they are nearly aligned along a vector of ~3.4 kpc long, perpendicular to this solar centered circle. This justifies our interest to study them in the context of the local structure and evolution of the Galactic disc. We chose to focus on the local disc properties rather than on a global analysis of the entire Galactic disc in that region because, given the complexity of the Galactic disc, the addition of only three clusters to those known in this field does not represent a statistically significant cluster sample which may render new results. However, the spatial distribution of the studied clusters allows us to examine if there exists any connection among their fundamental parameters, if we consider their Galactic longitude dependence. Moreover, a first analysis can be made if we estimate representative mean values of the interstellar visual absorption, of the age and of the metallicity in the neighborhood of each cluster and instead of using the individual values derived for the three clusters, we look for any relation between these mean values and the Galactic longitude. Thus, on the basis of these results and others from well-known OCs in the region, we could later deal with other issues such us whether the clusters were formed at the positions currently observed, whether there is any cluster to cluster variation in the interstellar extinction law, whether the radial metal abundance gradient varies with the Galactic longitude and so on.

In order to estimate the average values of the interstellar visual absorption, the age and the metallicity and their corresponding dispersions in the vicinity of each cluster, we decided to consider the clusters within a sphere of radius of 1 kpc centered on each of the three studied OCs. We think that such spherical volume is meaningful from a physical point of view because it is large enough to include a significant number of well-studied OCs. Furthermore, such volumen can be regarded as a representative region of the Galactic disc. Remember that the most frequently used value for the Galactocentric distance is 8.5 kpc. This means that the chosen spherical volume centered in each of our three OCs has a radius which represents ~10% of the Sun's Galactocentric distance. On the other hand, the maximum difference between the heights out of the Galactic plane of Czernik 26, Czernik 30, and Haffner 11 is 1.21 kpc, which means that the chosen spheres (1 kpc in radius) cover practically the same Z range for the three clusters.

We used the WEBDA open cluster database (Mermilliod and Paunzen, 2003) with the aim of selecting clusters located within ~1 kpc around Czernik 26, Czernik 30, and Haffner 11. We decided to use WEBDA for it is periodically updated, thus being an excellent tool to analyze cluster samples. Table 7 lists the selected clusters

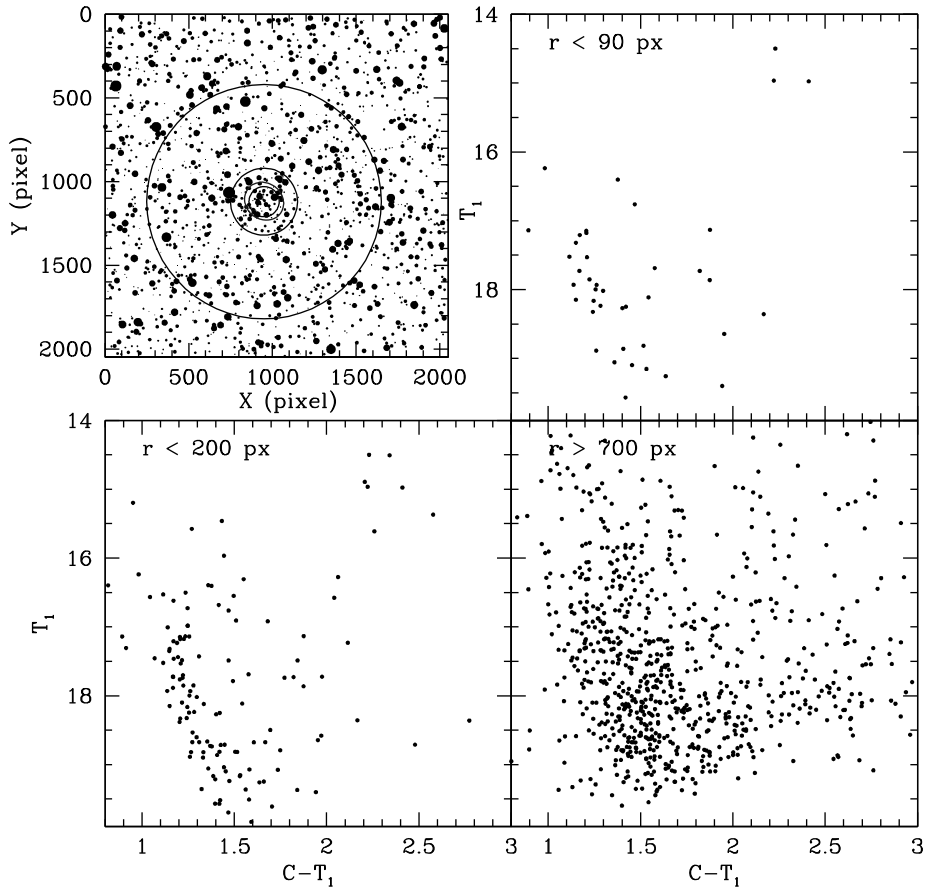

Fig. 4. Same as Fig. 3, for Czernik 30.

from WEBDA which verify the above stated requirement. Notice that since we are interested in estimating the mean values of the interstellar absorption, the age, and the metalliciy at the three cluster positions, such list includes a limited number of OCs. WEBDA provides the $E(B-V)$ color excess, distance from the Sun and age for all the selected clusters, with the only exception of Waterloo 3 whose age is not given. Unfortunately, metal content has not been estimated for any of them. All in all, three OCs with known fundamental parameters were found around Czernik 26 and Czernik 30, while four OCs are seen around Haffner 11. In any case, we believe that further research is required to increase the number of detailed studies on Galactic OCs.

The upper panels of Fig. 7 show the distribution of the clusters in different Galactic coordinate planes. Czernik 26, Czernik 30, and Haffner 11 are represented by a filled box, circle, and triangle, respectively, while the clusters located around them are represented using open same-shaped symbols. In addition, we have drawn solar centered circles of radii 5 and 8 kpc in the upper right-hand panel and marked the Perseus spiral arm according to Drimmel and Spergel (2001). Note that all the clusters are distributed around the Galactic plane (see upper left-hand panel). Note also that the smaller the mean Galactic longitude of a cluster group, the larger the dispersion in Galactic latitude. Bearing in mind that Czernik 26, Czernik 30, and Haffner 11 are at approximately the same distance from the Sun, the distribution of OCs in the (l,b) plane implies that the larger the mean Galactic longitude of a cluster group, the smaller the intrinsic volume occupied by them in the disc. We want to point out that we have searched only for OCs within regions of a fixed spherical volume (1 kpc in radius). Since clusters with larger Galactic longitudes are closer to or inside the Perseus spiral arm (see upper right-hand panel), they are likely to have been formed in that spiral arm. On the other hand, clusters at smaller Galactic longitudes are situated farther from the Perseus spiral so they could have been born in the disc, which has a larger height scale, compatible with more dispersion in Galactic latitude.

As far as the distribution of dust in front of the selected OCs is concerned, we first note that the closer a cluster to the Perseus spiral arm, the larger its interstellar visual absorption A_V, as can be clearly seen in the three filled symbols of the bottom left-hand panel of Fig. 7. Note that all the selected clusters lie behind the Perseus spiral arm. Thus, the group of clusters around Haffner 11 (triangles) have on average the highest interstellar visual absorption value, if compared with the mean values of the other two groups (circles and boxes). Particularly, the dispersion between the different interstellar extinction values of clusters in the Haffner's group reflects the inhomegeneity of the dust distribution throughout the Perseus spiral arm. On the other hand, the group of clusters around Czernik 26 exhibit the lowest average A_V value. Its larger dispersion, however, is probably due to the fact that two clusters of this group are close to the Galactic plane ($b \approx 0°$), while two other clusters are at $|b| > 6°$ as shown in the upper left-hand panel of Fig. 7. Once again, it is confirmed that the presence of the Perseus spiral arm affects the behavior of the A_V values along the cluster directions. In general, we confirm that the larger the height out the Galactic plane, the lower the interstellar visual absorption A_V. However, since OCs lie in the Galactic disc, it is to be expected that they are sometimes affected by high and/or irregular interstellar extinctions, as pointed out by Piskunov et al. (2006). For example, according to Bonatto et al. (2006), the distribution of reddenings of

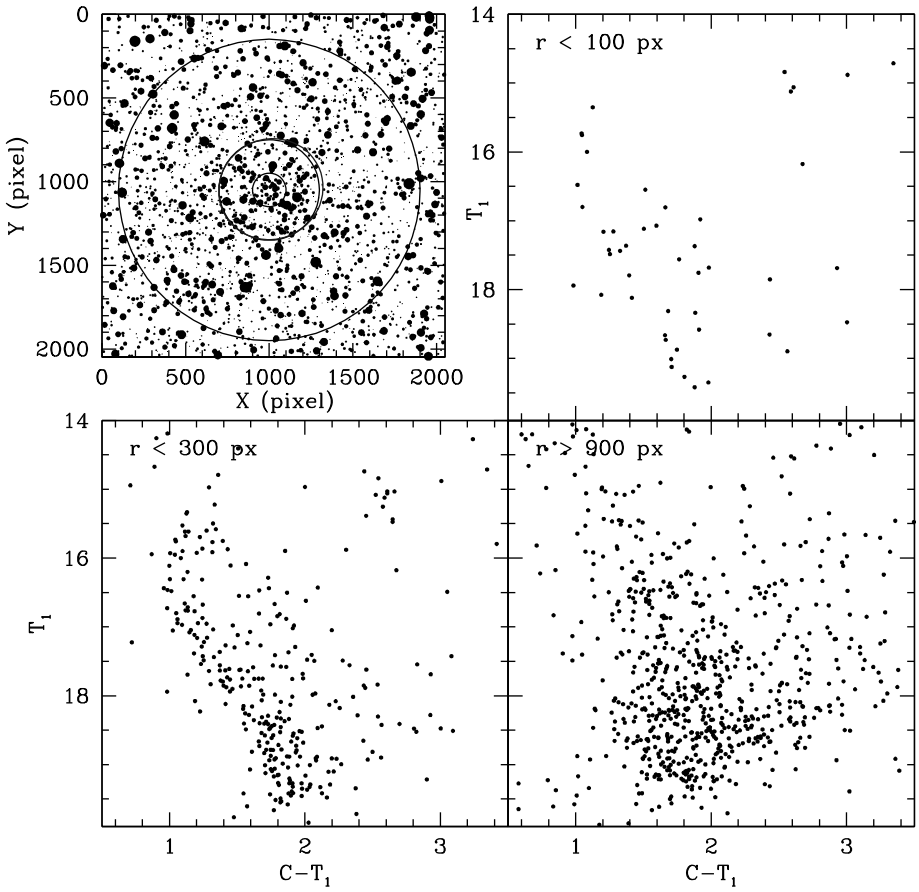

Fig. 5. Same as Fig. 3, for Haffner 11.

young clusters is broader than that of the intermediate-age and old clusters. This is probably due to the fact that young clusters are affected by a greater internal reddening. Besides, young clusters are affected by higher reddenings because they are more concentrated towards the Galactic plane. Bonatto et al. showed that $E(B-V)$ increases nearly linearly with the heliocentric distance up to $\simeq$3 kpc. The dispersion in the $E(B-V)$ values appears to be significantly larger for longer distances.

Finally, we examined the distribution of cluster ages as a function of cluster heights out of the Galactic plane (Z). In the bottom right-hand panel of Fig. 7, we show the relation we found between these two parameters. The clusters around Haffner 11 (open triangles) are all very young and possibly they have not had chance of moving far from their birthplaces. So, it is probable that they were formed in the Perseus spiral arm judging from their current positions, as can be seen in the upper right-hand panel. Since Haffner 11 is $\sim$0.5 Gyr old, we infer that it was not formed together with the other clusters of the group, although it is located in the disc near the Perseus spiral arm. In the case of the clusters around Czernik 30, one of them is located at $b \approx 0^\circ$ and is very young, while the other two are intermediate-age or old clusters situated out of the Galactic plane (see Table 7). With such age dispersion, we believe that Czernik 30 was not born near the Galactic plane, where it is now observed, but in the Galactic disc. Lastly, the same as for the clusters around Czernik 30, a large age and Galactic latitude dispersion is observed for the clusters around Czernik 26. This fact tends to favor the formation of Czernik 26 out of the Galactic plane.

It can be concluded from this analysis that the cluster velocity dispersion perpendicular to the Galactic plane in the spiral arms as well as in the Galactic plane is, in general, smaller than in the Galactic disc. Unless a cluster born in the Galactic plane does have a high W space velocity perpendicular to the Galactic disc, it is bound to oscillate within a small range of Z height scales. Conversely, OCs born in the disc can either be formed at larger Z values or can reach such values as a consequence of their orbital motions (Piatti et al., 1995). These OCs generally have a larger W space velocity dispersion than those born in the plane. Consequently, they also reach larger Z values. Furthermore, if these OCs were also relatively old, they must have had the chance to cross the Galactic plane several times in their lifetimes so that we could find them at any Z value. Such value can be very different from that the clusters had when they were formed. For this reason, we believe it is worth enlarging our knowledge of the clusters' birthplaces for a comprehensive study of the metal abundance gradient perpendicular to the Galactic plane. In order to achieve this aim, it would be necessary to increase the number of OCs with mean proper motions and radial velocities accurately determined. Indeed, having these data available, it would be possible to compute their Galactic orbits backwards in time (Tecce et al., 2006).

As shown by Martin et al. (2004a), Bellazzini et al. (2004) and Bellazzini et al. (2006), the recently discovered CMa structure appears as the strongest spatial overdensity of the whole Galactic disc in terms of either number density or statistical significance. The structure appears elongated along the tangential direction, extending from $l \approx 200^\circ$ to $l \approx 280^\circ$. The evidences collected by Martin et al. (2004a,b), Martínez-Delgado et al. (2005), Bellazzini et al. (2006) are clearly explained by the hypothesis of a disrupting dwarf galaxy in a nearly circular and nearly planar orbit around the center of the Galaxy.

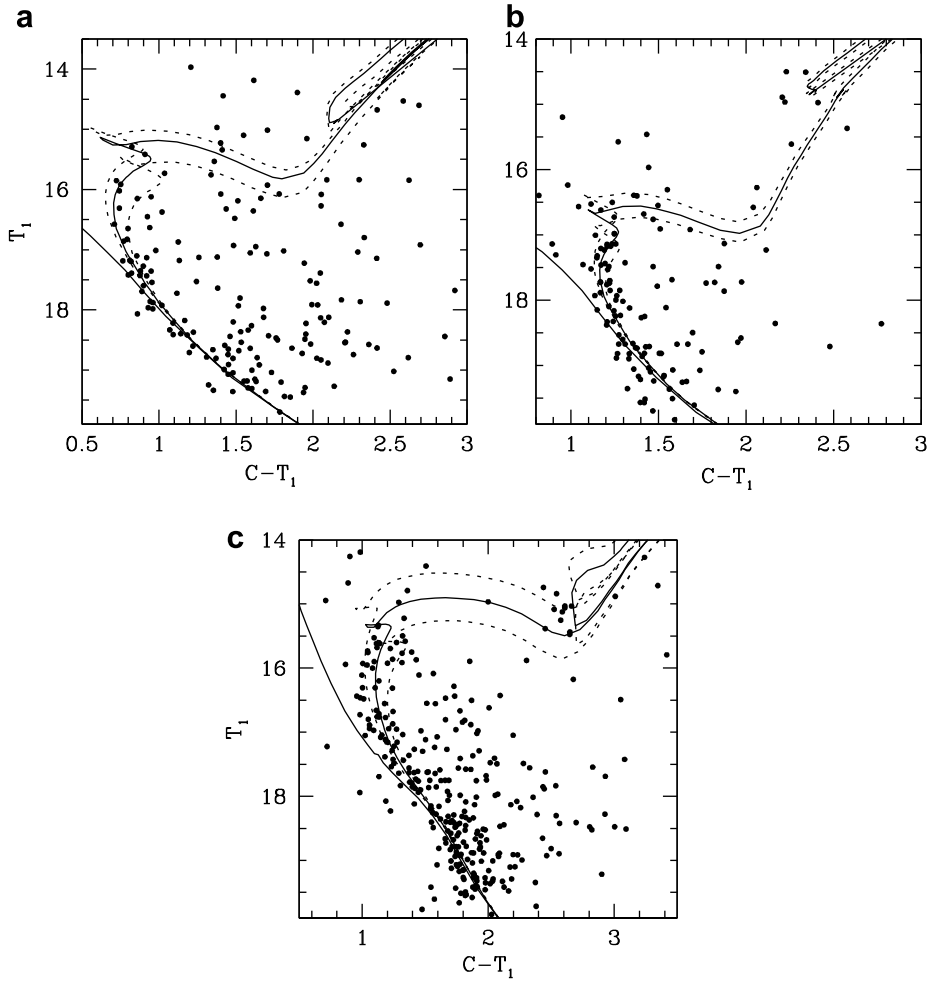

Fig. 6. $r < r_{clean}$ ($C - T_1$, T_1) CMDs for stars in: (a) Czernik 26; (b) Czernik 30; and (c) Haffner 11. The ZAMS and the adopted isochrones from Girardi et al. (2002), computed taking into account overshooting (see Table 7), are overplotted with solid lines. We included in dashed lines the isochrones associated to the cluster age errors, for comparison purposes.

Table 6
Fundamental parameters of the selected clusters

Name	$E(B-V)$ (magnitude)	d (kpc)	Age (Gyr)	[Fe/H] (kpc)	X (kpc)	Y (kpc)	Z (kpc)	R_{GC}
Czernik 26	0.05 ± 0.05	6.7 ± 1.4	$1.30^{+0.16}_{-0.13}$	0.0 ± 0.2	13.997	−3.756	−0.759	14.532
Czernik 30	0.26 ± 0.02	6.2 ± 0.8	$2.50^{+0.30}_{-0.25}$	−0.4 ± 0.2	12.767	−4.476	0.451	13.543
Haffner 11	0.57 ± 0.05	6.1 ± 1.1	$0.50^{+0.13}_{-0.10}$	−0.4 ± 0.2	11.321	−5.395	−0.377	12.550

Table 7
Fundamental parameters for clusters located within 1 kpc from Czernik 26, Czernik 30, and Haffner 11, respectively

Cluster	l (°)	b (°)	$E(B-V)$ (magnitude)	d (kpc)	Age (Gyr)	Z (kpc)	R_{GC} (kpc)
Dolidze 25	211.942	−1.273	0.72	6.30	0.07	−0.14	14.25
Berkeley 34	213.731	2.108	0.45	7.28	2.80	0.24	15.11
Berkeley 73	215.278	−9.424	0.10	6.85	2.29	−1.12	14.64
Berkeley 33	225.424	−4.622	0.30	7.00	0.79	−0.56	14.31
Berkeley 36	227.376	−0.587	0.40	6.14	3.16	−0.06	13.44
NGC 2401	229.665	1.854	0.36	6.30	0.03	0.20	13.46
Ruprecht 32	241.566	−0.573	0.50	5.35	0.01	−0.05	12.00
Waterloo 3	242.562	1.444	0.34	5.20	–	0.13	11.83
Haffner 19	243.081	0.524	0.42	5.09	0.01	0.05	11.72
Haffner 18	243.151	0.447	0.61	6.03	0.01	0.05	12.44

We took advantage of the fact that the studied OCs are projected in the direction to the CMa dwarf galaxy (Martin et al., 2004a) to explore whether there is any physical connection between them. We did so by comparing their positions, interstellar visual absorptions, ages, and metallicities. For the CMa galaxy, we adopted age and [Fe/H] ranges between ∼4 and 10 Gyr

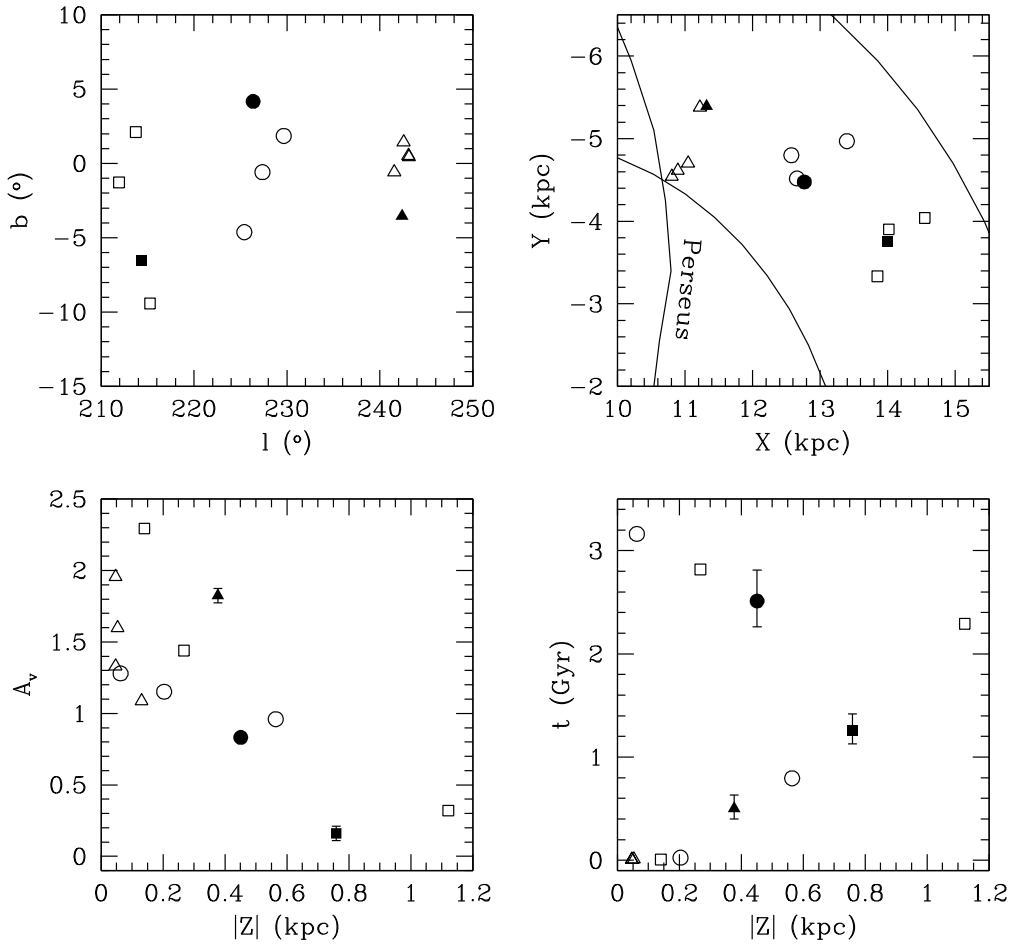

Fig. 7. Relationships between the Galactic coordinates l and b (upper left), between the Galactic coordinates X and Y (upper right), between the interstellar visual absorption A_V and the height $|Z|$ out of the Galactic plane (bottom right), and between the age and $|Z|$ for known open clusters placed within 1 kpc around Czernik 26 (box), Czernik 30 (circle), and Haffner 11 (triangle). Selected known clusters and presently studied clusters are represented by filled and open symbols, respectively. Sun centered circles of radii 5 and 8 kpc are shown in the upper right-hand panel, while the errorbars for A_V and age are shown in the bottom left and bottom right panels, respectively.

and −0.3 and −0.7 dex, respectively, for its main population (Bellazzini et al., 2004; Martínez-Delgado et al., 2005) and $E(B-V) = 0.08 \pm 0.07$. The position of the CMa main body centered at $(l, b) = (240, -8)$ (Martínez-Delgado et al., 2005) and the region ascribed to the galaxy according to Bellazzini et al. (2006) are schematically represented by solid contours in Fig. 8. We included in this figure the three studied OCs and those from Table 7. Note that although Czernik 26, Czernik 30, and Haffner 11 are located within the relevant heliocentric distances and Galactic longitudes ascribed to CMa (see right panel), their Galactic latitudes show that

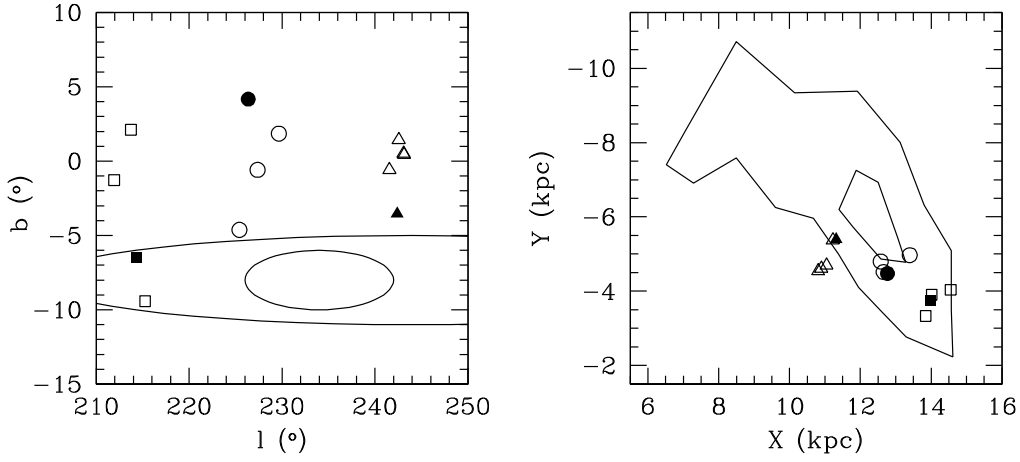

Fig. 8. Relationships between the Galactic coordinates l and b (left) and between the Galactic coordinates X and Y (right) for the clusters of Table 7. The inner and outer contours represent schematic limits of the main body and the region ascribed to CMa, respectively, as taken from Martínez-Delgado et al. (2005), Bellazzini et al. (2004), Bellazzini et al. (2006). Symbols are as in Fig. 7.

Table 8
Probability criteria of the relationship between the studied clusters and CMa

Cluster	CMa attributable region	CMa main body	$E(B-V)$	Age	[Fe/H]	Adopted
Czernik 26	Yes	No	Yes	No	No	No
Czernik 30	No	No	No	No	Yes	No
Haffner 11	No	No	No	No	Yes	No

only Czernik 26 is located within what is considered the CMa region, while Haffner 11 is marginally located onto CMa and Czernik 30 lies in its surroundings.

Martin et al. (2004a) also searched the WEBDA database for OCs located in the region of the CMa overdensity. They argued that since the heliocentric distances of the two young OCs-Dolidze 25 and Haffner 18 (log(age) < 8.5) – and of the old cluster Arp-Madore 2 are compatible with the distance to CMa, these three OCs could have formed as a result of an enhanced star formation activity in the disc. Bellazzini et al. (2004) reviewed their search with the aim of confirming the existence of an apparent overdensity of OCs in the surroundings of CMa (Martin et al., 2004a). They also showed that only the old and relatively metal-poor OCs Arp-Madore 2 and Tombaugh 2 have positions, ages, and metallicities within the range ascribed to the main body of CMa. More recently, Bellazzini et al. (2006) determined the heliocentric distances of Tombaugh 2, Arp-Madore 2, and Haffner 11 and concluded that these three OCs are physically located within the main body of CMa. They did not find in the WEBDA database any other cluster located in the CMa region and its surroundings. Further research is therefore needed to confirm the existence of such group of OCs related to CMa.

On the other hand, the three studied OCs happen to be much younger than the CMa main population, while their metal abundances lean towards the metal-rich end of the metallicity distribution of CMa. In this sense, it would seem unlikely that these objects were born in CMa before this dwarf galaxy was accreted by the Milky Way. In addition, only two clusters – Czernik 26 and Berkeley 73 – share similar interstellar visual absorptions within the expected range towards CMa. Bellazzini et al. (2004) showed that there is a sparse population of younger stars of $\leqslant$1–2 Gyr that is also associated with the CMa overdensity. De Jong et al. (2007) found that these young stars are at least a few hundred million years old and at most 2 Gyr. Although the degeneracy between distance and metallicity prevented De Jong et al. from drawing a firm conclusion about the co-spatiality of the old and young stars, a metal-rich ([Fe/H] $\simeq -0.3$) population at $\sim$9.3 kpc and a metal-poor ([Fe/H] $\simeq -0.8$) population at 7.5 kpc are both consistent with their data. Carraro et al. (2008) found that the spatial distribution of the stars younger than 100 Myr peaks at a heliocentric distance of $9.8^{+1.5}_{-1.0}$. They claim that these young stars are expected to be found because of the warped spiral structure of the Galactic disc in the region. It is therefore unnecessary to postulate the existence of an accreted dwarf galaxy in CMa to find them. Czernik 26, Czernik 30, and Haffner 11 are located much closer to the Sun than $\sim$10 kpc and are older than 100 Myr.

We have used here as physical connection criteria, among the studied OCs and CMa, the comparison not only between their positions but also between their interstellar visual absorptions, ages and metallicities (Table 6). Table 8 summarizes the resulting probabilities of the relationships between these three OCs and CMa. The results of the current study tend to support the hypothesis that the three studied OCs belong to the Galactic disc.

5. Summary

In this paper, we present CCD CT_1 Washington photometry in the fields of the southern low-contrast OCs Czernik 26, Czernik 30, and Haffner 11. The analysis of the photometric data leads to the following main conclusions:

(i) The observed $(C-T_1, T_1)$ diagrams reveal that there is a high field star contamination in the three observed fields. To disentagle cluster features from those belonging to their surrounding fields, we traced their stellar density radial profiles to derive the cluster radii. The three clusters turned out to be relatively small angular sized objects.

(ii) After a thorough analysis of their radial density profiles, we estimated the percentage of field star contamination as a function of the distance from each cluster's center. Field star contamination rises from 25% up to 55% at a distance corresponding to half the maximum of the cluster stellar density profile. The number of field star reaches 50–65% at a radius which represents a compromise between maximizing the number of cluster stars and minimizing the number of field stars, while it goes up to 60–90% at the cluster radius.

(iii) The comparison of the cluster $(C-T_1, T_1)$ CMDs with theoretical isochrones computed by the Padova group yielded the cluster $E(B-V)$ color excesses, distances from the Sun and ages. It also permitted to estimate acceptable ranges of metallicity for each cluster. Czernik 26 is found to be located within what is considered the CMa region, while Haffner 11 is marginally located onto CMa and Czernik 30 lies in its surroundings. Evidence is presented to favor the hypothesis that these three OCs are not related to CMa but belong to the Galactic disc.

(iv) Using the WEBDA open cluster database to search for OCs with well-known fundamental parameters situated around 1 kpc from the centers of Czernik 26, Czernik 30, and Haffner 11, we examined the relationships between their ages, their interstellar visual absorptions and their positions in the disc. We found that the closer the cluster birthplaces to the Galactic plane, the higher the interstellar visual absorption. We also found that the space velocity dispersion perpendicular to the Galactic plane diminishes as the clusters are younger.

Acknowledgements

We are gratefully indebted to the CTIO staff for their hospitality and support during the observing run. We would like to thank the anonymous referee for their helpful comments and suggestions which contributed to the improvement of this manuscript. The present work was partially supported by the Argentinian institutions CONICET and SECYT (Universidad Nacional de Córdoba). This work is based on observations made at Cerro Tololo Inter-American Observatory (CTIO), which is operated by AURA Inc., under cooperative agreement with the National Science Foundation.

References

Bellazzini, M., Ibata, R., Monaco, L., Martin, N., Irwin, M.J., Lewis, G.F., 2004. MNRAS 354, 1263.
Bellazzini, M., Ibata, R., Martin, N., Lewis, G.F., Conn, B., Irwin, M.J., 2006. MNRAS 366, 865.
Bica, E., Bonatto, C., 2005. A&A 465, 475.
Bonatto, C., Kerber, L.O., Bica, E., Santiago, B.X., 2006. A&A 446, 121.
Canterna, R., 1976. AJ 81, 228.

Carraro, G., Moitinho, A., Vázquez, A., 2008. arXiv:0801.2084.
Clariá, J.J., Piatti, A.E., Parisi, M.C., Ahumada, A.V., 2007. MNRAS 379, 159.
De Jong, J.T.A., Butler, D.J., Rix, H.-W., Dolphin, A.E., Martínez-Delgado, D., 2007. ApJ 662, 259.
Dias, W., Alessi, B.S., Moitinho, A., Lepine, J.R.D., 2002. A&AS 141, 371.
Drimmel, R., Spergel, D.N., 2001. ApJ 556, 181.
Geisler, D., 1996. AJ 111, 480.
Girardi, L., Bertelli, G., Bressan, A., Chiosi, C., Groenewegen, M.A.T., et al., 2002. A&A 391, 195.
King, I., 1962. AJ 67, 471.
Lauberts, A., 1982, ESO/Uppsala Survey of the ESO(B) Atlas. ESO, Garching.
Lejeune, T., Schaerer, D., 2001. A&A 366, 538.
Martin, N., Ibata, R.A., Bellazzini, M., Irwin, M.J., Lewis, G.F., Dehnen, W., 2004a. MNRAS 348, 12.
Martin, N., Ibata, R.A., Conn, B., Lewis, G.F., et al., 2004b. MNRAS 355, L33.
Martínez-Delgado, D., Butler, D.J., Rix, H.-W., Franco, I., et al., 2005. ApJ 633, 205.
Mermilliod, J.-C., Paunzen, E., 2003. WEBDA open cluster database. A&A 410, 511.
Piatti, A.E., Bica, E., Geisler, D., Clariá, J.J., 2003. MNRAS 344, 965.
Piatti, A.E., Clariá, J.J., Abadi, M.G., 1995. AJ 110, 2813.
Piatti, A.E., Clariá, J.J., Ahumada, A.V., 2003. MNRAS 340, 1249.
Piatti, A.E., Clariá, J.J., Ahumada, A.V., 2004. A&A 421, 991.
Piatti, A.E., Sarajedini, A., Geisler, D., Clark, D., Seguel, J., 2007. MNRAS 377, 300.
Piskunov, A.E., Kharchenko, N.V., Röser, S., Schilbach, E., Scholz, R.-D., 2006. A&A 445, 545.
Piskunov, A.E., Schilbach, E., Kharchenko, N.V., Röser, S., Scholz, R.-D., 2008. A&A 477, 165.
Stetson, P.B., Davis, L.E., Crabtree, D.R., 1990. In: AS Conf. Ser. 8, CCDs in Astronomy. ASP, San Francisco, p. 289.
Tecce, T.E., Pellizza, L.J., Piatti, A.E., 2006. Rev. Mex. A. A. Conf. Series 26, 86.
van den Bergh, S., Hagen, G.L., 1975. AJ 80, 11.